Cooperative Optimal Multi-Robot Formation Arrangement for Object Pushing

Hung Pham Quang and Hung Pham Duy

[1] VietNam National University, HaNoi, VietNam
hungpq.uet@vnu.edu.vn
[2] VietNam National University, HaNoi, VietNam
hungpd@vnu.edu.vn

Abstract. This paper presents a methodology for determining optimal pushing force placements and designing a simple controller for trajectory tracking of rigid objects. The objective is to address the challenge of manipulating objects using only pushing forces under frictional constraints. A Particle Swarm Optimization (PSO) framework is proposed to determine the optimal placement of pushing forces on the object boundary. The optimization objective integrates multiple criteria derived from grasp and Gram matrix analysis, ensures generate a wide range of wrench to handle diverse manipulation tasks and uniform distribution of pushing directions. These criteria are combined into a comprehensive cost function that guides the swarm toward configurations that ensure stability and controllability. Once the pushing positions are determined, a simple PID-based controller is employed to generate the desired wrench for path tracking. The simulation results demonstrate that the strategy has produced suitable contact point locations and provided efficiency and stability in the process of pushing the object. The combined approach offers a practical and computationally efficient framework for pushing-based manipulation, with potential applications in robotic handling of objects that cannot be grasped.

Keywords: Pushing-based manipulation; Particle Swarm Optimization; Force posititon; PID control; Wrench space; Robotic path tracking

1 Introduction

Currently, handling heavy or bulky objects often requires non-grasping strategies such as pushing, due to limitations of grippers or environmental constraints [5–7]. In such scenarios, multiple robots may need to cooperate to transport large or heavy objects, for instance, in warehouse logistics or rescue operations, where a single robot cannot accomplish the task alone [4]. This problem has recently attracted significant attention in robotic manipulation, particularly in the context of multi-robot systems.

Pushing-based manipulation [9, 11] has become an important research topic in multi-robot systems, especially when dealing with objects that are too large, heavy, or cumbersome to be grasped directly. Instead of relying on traditional

grippers, robots can interact with objects by applying external pushing forces along their boundaries. This approach is attractive because it requires force mechanisms, yet it also introduces significant challenges. The dynamics of rigid objects under pushing are inherently non-linear and subject to non-holonomic constraints, while the feasible interaction forces are strictly limited by Coulomb friction cones. Consequently, ensuring stability and precise path tracking through using pushing-only strategies remains a nontrivial problem.

In general, pushing-only object manipulation can be divided into two complementary stages: (i) determining the configuration of contact points that apply pushing forces to the object, and (ii) controlling these forces to move the object along the desired trajectory. This paper focuses primarily on the first stage - the optimization of pushing force positions. Identifying sufficiently good positions not only ensures controllability but also significantly reduces the burden on the subsequent force control stage. Once optimal positions are obtained, a simple controller is sufficient to achieve stable trajectory tracking.

The mechanics of pushing were first rigorously studied by Lynch [8], who introduced the concepts of motion cones and limit surfaces to describe how frictional contacts govern the object motion. This work laid the foundation for understanding nonprehensile manipulation, but it remained largely analytical and did not address the problem of selecting or optimizing contact locations. Bertoncelli et al. [1] proposed a task-oriented optimization of contact locations for cooperative pushing with mobile robots. Their method focuses on minimizing the required pushing forces during trajectory execution, demonstrating the benefits of carefully chosen contact points. However, their approach is tailored to multi-robot settings and primarily considers force minimization rather than controllability or isotropy of the wrench space. Fujisawa et al. [3] investigated cooperative transport strategies inspired by ant foraging behavior. They proposed artificial pheromone communication to coordinate robots during pushing. An straightforward solution in their work is to have all robots push in the same direction, distributed behind the object. Although this setup simplifies the coordination, it inherently limits perception since no individual robot maintains a complete view of the environment. Furthermore, such strategies do not explicitly optimize the placement of pushing forces with respect to controllability or stability, but instead rely on uniform alignment. Tang et al. [10] proposed a comprehensive framework for collaborative planar pushing of polytopic objects in cluttered environments, combining mode generation, hybrid search, and non-linear model predictive control. Their approach introduces a sparse optimization scheme (MG-SO) to select effective contact points and evaluates them using multi-directional feasibility metrics under quasistatic analyses. While this framework is scalable and complete under mild assumptions, its evaluation criteria do not directly reflect controllability or wrench space shape. Ebel et al. [2] addressed the problem of finding suitable formations for mobile robots to transport objects by pushing. Their approach explicitly considers the non-prehensile nature of the task and investigates how robot formations influence the success of object delivery. This work highlights the importance of the initial arrangement

of robots around the object, showing that formation design directly impacts controllability and task completion.

While these works demonstrate the richness of pushing as a non-prehensile manipulation paradigm, most either assume contact points are given and focus on control, or rely on heuristic feasibility-based contact selection. In contrast, our work concentrates on the often overlooked first phase of pushing manipulation: optimization of pushing force positions. Identifying sufficiently good positions not only guarantee controllability, but also substantially reduce the complexity of the subsequent control phase. To this end, we introduce algebraically motivated quality indices derived from the Gram matrix. We employ Partical Swarm Optimization (PSO) algorithm to search for positions that maximize these indices under physical constraints and validate the results using a simple controller.

The remainder of this paper is organized as follows. Section II overviews rigid-body object dynamics. Section III outlines the problem and objectives. Section IV present the proposed approach. Section V discusses the results of both simulation and real-world experiments.Finally, the conclusions are presented in Section VI.

2 Background

2.1 Rigid Body and Quasi-Static Dynamic Models

Consider a rigid object moving on a planar surface under the influence of multiple contact forces applied by robotic manipulators or pushing mechanisms. The object is described by the vector $\mathbf{q} = [x, y, \theta]^T \in \mathbb{R}^2 \times S^1$, where (x, y) represents the position of the center of mass in the global coordinate frame, and θ denotes the orientation of the object.

Using Newton's law of motion and Euler's rigid-body equation, the dynamics of the system are given as follows:

$$\mathbf{M}\ddot{\mathbf{q}} + \mathbf{B}\dot{\mathbf{q}} = \mathbf{w} \tag{1}$$

where $\mathbf{M} \in \mathbb{R}^{3\times3}$ is the inertia matrix, $\mathbf{B} \in \mathbb{R}^{3\times3}$ represents the effective friction matrix, and $\mathbf{w} = [f_x, f_y, \tau]^T \in \mathbb{R}^3$ represents the net wrench applied to the object.

In typical manipulation scenarios with high surface friction ($\mathbf{B}$ large) and relatively low velocities, the inertial effects are negligible compared to the friction forces. In such cases, the dynamics to be approximated using a quasi-static model:

$$\dot{\mathbf{q}} = \mathbf{B}^{-1}\mathbf{w} \tag{2}$$

This approximation significantly simplifies the control problem while maintaining sufficient accuracy for most practical applications.

2.2 Contact Force Model and Friction Constraints

Each contact force $\mathbf{f}_i$ applied at point P_i can be decomposed into components along the local contact frame:

$$\mathbf{f}_i = \alpha_i \mathbf{n}_i + \beta_i \mathbf{t}_i \tag{3}$$

where $\mathbf{n}_i = [n_{ix}, n_{iy}]^T$ is the unit inward normal vector at the contact point, $\mathbf{t}_i = [t_{ix}, t_{iy}]^T = [-n_{iy}, n_{ix}]^T$ is the unit tangential vector perpendicular to $\mathbf{n}_i$, $\alpha_i \geq 0$ is the normal force magnitude (push-only constraint), and β_i is the tangential friction force magnitude.

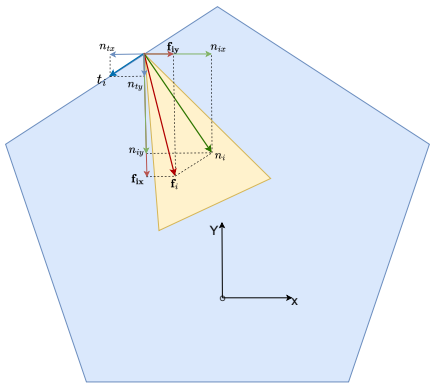

Fig. 1: Contact force model at point P_i. The friction cone constraint limits the ratio between tangential and normal force components.

Coulomb friction constraint: The tangential force at each contact point is bounded by the friction cone:

$$|\beta_i| \leq \mu_i \alpha_i, \quad \forall i = 1, 2, \ldots, n \tag{4}$$

where μ_i is the coefficient of friction at contact point i. This constraint defines a friction cone in the force space, within which all feasible contact forces must lie.

2.3 Wrench Space Representation and Grasp Matrix

The relationship between individual contact forces and the net wrench acting on the object's center of mass is derived from kinematic analysis. For a contact force $\mathbf{f}_i = [f_{ix}, f_{iy}]^T$ applied at point P_i with a position vector $\mathbf{r}_i = [r_{ix}, r_{iy}]^T$ relative to the center of mass, the corresponding wrench contribution is:

$$\mathbf{w}_i = \begin{bmatrix} f_{ix} \\ f_{iy} \\ r_{ix} f_{iy} - r_{iy} f_{ix} \end{bmatrix} \tag{5}$$

Substituting the force decomposition from (3) and simplifying gives:

$$\mathbf{w}_i = \begin{bmatrix} \alpha_i n_{ix} - \beta_i n_{iy} \\ \alpha_i n_{iy} + \beta_i n_{ix} \\ \alpha_i A_i + \beta_i B_i \end{bmatrix} \tag{6}$$

where $A_i = r_{ix} n_{iy} - r_{iy} n_{ix}$ and $B_i = r_{ix} n_{ix} + r_{iy} n_{iy}$ are the moment arm coefficients. The total wrench is the sum of all individual contributions: $\mathbf{w} = \sum_{i=1}^{n} \mathbf{w}_i$. This relationship can be expressed in matrix form as follows:

$$\mathbf{w} = \mathbf{G}\mathbf{x} \tag{7}$$

where $\mathbf{x} = [\alpha_1, \beta_1, \alpha_2, \beta_2, \ldots, \alpha_n, \beta_n]^T \in \mathbb{R}^{2n}$ is the force parameter vector and the extended grasp matrix $\mathbf{G}' \in \mathbb{R}^{3\times 2n}$ has the structure:

$$\mathbf{G} = \begin{bmatrix} n_{1x} & -n_{1y} & n_{2x} & -n_{2y} & \cdots & n_{nx} & -n_{ny} \\ n_{1y} & n_{1x} & n_{2y} & n_{2x} & \cdots & n_{ny} & n_{nx} \\ A_1 & B_1 & A_2 & B_2 & \cdots & A_n & B_n \end{bmatrix} \tag{8}$$

The feasible wrench space $\mathcal{W}_f$ represents the set of all wrenches that can be generated while respecting the physical constraints:

$$\mathcal{W}_f = \{\mathbf{w} \in \mathbb{R}^3 : \mathbf{w} = \mathbf{G}\mathbf{x}, \mathbf{x} \in \mathcal{X}_f\} \tag{9}$$

where the feasible force parameter space is defined as:

$$\mathcal{X}_f = \{\mathbf{x} \in \mathbb{R}^{2n} : \alpha_i > 0, |\beta_i| \leq \mu_i \alpha_i, \forall i = 1, 2, \ldots, n\} \tag{10}$$

The geometric properties of this wrench space, particularly those revealed through singular value decomposition of the grasp matrix $\mathbf{G}$, provide fundamental insights into the manipulation capabilities and limitations of different contact configurations. These properties form the mathematical basic for defining quantitative quality metrics that enable systematic optimization of contact point placement.

2.4 Contraint between robot and object surface

When a robot make contact with an object, an interaction force arises at the contact point. This force consists of a normal component, perpendicular to the surface, and a tangential component due to friction. The admissible range of this interaction is described by the friction cone, whose axis is aligned with the surface normal and whose aperture is determined by the friction coefficient.

As long as the applied pushing force lies within this cone, the robot can effectively transmit the force to the object without slipping. However, if the force direction falls outside the friction cone, the contact will no longer hold, and the robot will slide along the surface instead of pushing the object.

3 Problem Description

Consider the problem of optimally positioning n contact points on a rigid object to enable effective object manipulation through pushing forces. Each contact point P_i is characterized by its position vector $\mathbf{r}_i = [r_{ix}, r_{iy}]^T$ relative to the object's center of mass, and its corresponding inward normal vector $\mathbf{n}_i = [n_{ix}, n_{iy}]^T$. The manipulation system must provide sufficient wrench capabilities across all degrees of freedom while respecting the physical constraints imposed by Coulomb friction and the push-only condition.

Within the quasi-static manipulation framework established in Section II, the contact force $\mathbf{f}_i$ at each point is expressed as $\mathbf{f}_i = \alpha_i \mathbf{n}_i + \beta_i \mathbf{t}_i$, where $\alpha_i > 0$ denotes the magnitude of the normal pushing force, and $|\beta_i| \leq \mu_i \alpha_i$ represents the friction constraint. The relationship between the individual contact forces and the net wrench is captured by the extended grasp matrix $\mathbf{G} \in \mathbb{R}^{3\times 2n}$, which maps the force parameter space to the wrench space via $\mathbf{w} = \mathbf{G}\mathbf{x}$.

A fundamental requirement for controllable manipulation is the ability to generate bidirectional moments about the object's center of mass. This capability is quantified by the moment arm coefficients $A_i = r_{ix} n_{iy} - r_{iy} n_{ix}$, which represents the rotational effect of normal forces at each contact point. For full controllability, there must exist at least one pair of contact points i and j such that $A_i \cdot A_j < 0$, ensuring that both clockwise and counterclockwise moments can be produced.

The primary challenge is to simultaneously optimize multiple conflicting objectives while satisfying the bidirectional moment constraint. Specifically, the system must address the following requirements:

- **T**he contact point configuration should generate a sufficiently wide range of wrenches to accommodate diverse manipulation tasks and external disturbances.
- **A**ll contact points must lie on the object boundary while ensuring the controllability condition $A_i \cdot A_j < 0$ is satisfied.

The moment arm coefficients A_i are inherently coupled with the contact geometry through the cross-product relationship $A_i = \mathbf{r}_i \times \mathbf{n}_i$. This coupling induces a complex interdependence between contact positions, surface normals, and the resulting manipulation capabilities, making analytical optimization intractable for arbitrary object geometries.

4 Methodology

To address the multi-objective optimization challenge identified in Section II, we propose a systematic framework that quantifies manipulation quality through mathematical metrics derived from the extended grasp matrix properties. The proposed methodology follows a two-phase approach as illustrated in Figure 2, which depicts the proposed two-phase system architecture. The offline optimization loop (top) consists of the PSO optimizer that processes object geometry

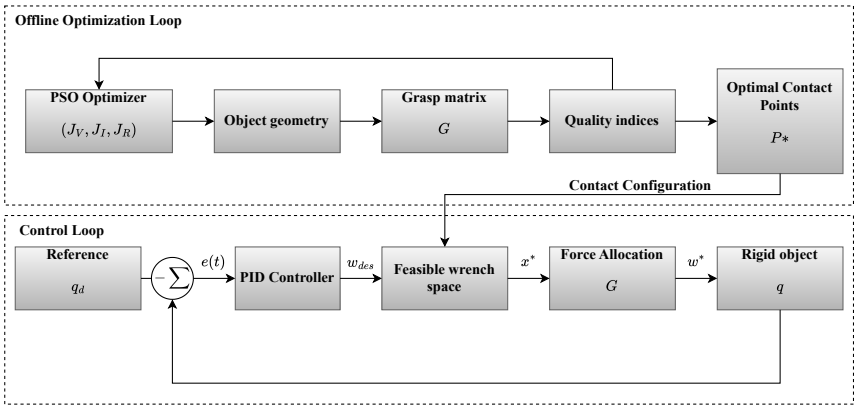

Fig. 2: System architecture overview

to determine optimal contact positions $P*$ by evaluating the grasp matrix G and quality indices (J_V, J_I, J_R). The online control loop (bottom) comprises a PID controller that computes the desired wrench w_{des} from the tracking error $e(t)$, a feasible wrench projection module that ensures physical constraints are satisfied, and a force allocation block that distributes forces to the multi-robot system. The optimal configuration $P*$ and the matrix G from the offline phase are passed to the online controller to define the feasible wrench space. Feedback $q(t)$ closes the control loop for continuous trajectory tracking.

4.1 Quality Indices from the Gram Matrix

The extended grasp matrix $\mathbf{G} \in \mathbb{R}^{3\times 2n}$, introduced in Section II, encapsulates the mapping between the contact points and the resulting wrench space. To analyze the manipulation capabilities inherent for a given contact configuration, we apply singular value decomposition:

$$\mathbf{G} = \mathbf{U}\mathbf{\Sigma}\mathbf{V}^T \tag{11}$$

where:

- $U = [u_1\ u_2\ u_3] \in \mathbb{R}^{3\times 3}$ and $V = [v_1\ v_2\ \dots\ v_{2n}] \in \mathbb{R}^{2n\times 2n}$ is an orthogonal matrix,
- $\Sigma \in \mathbb{R}^{3\times 2n}$ is an extended diagonal matrix containing the singular values $\sigma_1 \geq \sigma_2 \geq \sigma_3 \geq 0$

To understand this geometric relationship, consider a unit hypersphere in the force parameter space $\mathbb{R}^{2n}$, representing all possible normalized force combinations. When this unit hypersphere is mapped through the grasp matrix $\mathbf{G}$, it becomes stretched and transformed into an ellipsoid in the wrench space $\mathbb{R}^3$.

The singular values $\sigma_1, \sigma_2, \sigma_3$ represent the lengths of the ellipsoid's semiaxes along the principal directions.

The Gram matrix $\mathbf{W} = \mathbf{G}\mathbf{G}^T$ is directly related to the singular values through the decomposition.

$$\begin{aligned}\mathbf{W} &= \mathbf{G}\mathbf{G}^T && (12)\\ &= \mathbf{U}\mathbf{\Sigma}\mathbf{V}^T(\mathbf{U}\mathbf{\Sigma}\mathbf{V}^T)^T && (13)\\ &= \mathbf{U}\mathbf{\Sigma}\mathbf{V}^T\mathbf{V}\mathbf{\Sigma}^T\mathbf{U}^T && (14)\\ &= \mathbf{U}\mathbf{\Sigma}\mathbf{\Sigma}^T\mathbf{U}^T \quad (\text{since } \mathbf{V}^T\mathbf{V} = \mathbf{I}_{2n}) && (15)\end{aligned}$$

Multiplication of the matrix $\mathbf{\Sigma}\mathbf{\Sigma}^T$ results in:

$$\mathbf{\Sigma}\mathbf{\Sigma}^T = \begin{bmatrix}\sigma_1^2 & 0 & 0\\ 0 & \sigma_2^2 & 0\\ 0 & 0 & \sigma_3^2\end{bmatrix} \tag{16}$$

Therefore, the Gram matrix can be expressed as:

$$\mathbf{W} = \mathbf{U}\,\mathrm{diag}(\sigma_1^2, \sigma_2^2, \sigma_3^2)\,\mathbf{U}^T \tag{17}$$

Figure 3 illustrates the wrench space evaluation using Gram matrix analysis. The raw feasible wrench space (left) forms an irregular convex hull that provides limited geometric insight and makes systematic quality assessment challenging. In contrast, the ellipsoid representation obtained by the Gram matrix decomposition $W = GG^T$ (right) reveals a clear geometric structure with principal axes corresponding to singular values $\sigma_1, \sigma_2, \sigma_3$, allowing systematic computation of manipulation quality indices.

This transformation provides intuitive insight: instead of analyzing the complex, high-dimensional force parameter space directly, we can examine the simpler 3D wrench ellipsoid. The ellipsoid's volume indicates overall capability, its shape reveals directional preferences, and its smallest radius guarantees minimum performance. This geometric interpretation forms the foundation for our quality metrics. Based on the singular value analysis, we define three complementary quality metrics that capture distinct aspects of manipulation performance:

Volume Index (J_V): The volume index quantifies the overall manipulation capability by measuring the volume of the wrench ellipsoid:

$$J_V = \sigma_1\sigma_2\sigma_3 = \sqrt{\det(\mathbf{W})} \tag{18}$$

This metric represents the total amount of wrench space accessible to the manipulation system. Larger volumes indicate greater capability to handle diverse manipulation tasks and external disturbances.

Isotropy Index (J_I): The isotropy index measures the uniformity of force transmission characteristics:

$$J_I = \frac{\sigma_3}{\sigma_1} = \sqrt{\frac{\lambda_{\min}(\mathbf{W})}{\lambda_{\max}(\mathbf{W})}} \tag{19}$$

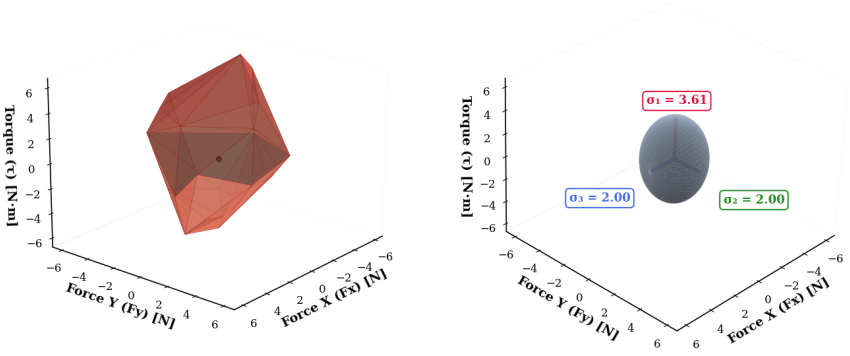

Fig. 3: Wrench space evaluation using Gram matrix analysis

This metric ranges from 0 to 1, with values closer to 1 indicating more uniform manipulation capabilities across all wrench directions. High isotropy ensures consistent performance and avoids weak manipulation axes.

Radius Index (J_R): The radius index represents the minimum guaranteed manipulation capability:

$$J_R = \sigma_3 = \sqrt{\lambda_{\min}(\mathbf{W})} \tag{20}$$

This metric defines the worst-case performance, ensuring adequate force generation capability even in the least favorable wrench direction.

These indices capture complementary aspects of manipulation quality and exhibit inherent trade-offs: configurations maximizing volume may sacrifice isotropy, while highly uniform configurations might have limited overall capability. The weighting coefficients in the optimization allow for task-specific emphasis on different performance aspects.

4.2 PSO-based Contact Point Optimization

Particle Swarm Optimization (PSO) is a population-based stochastic optimization algorithm. A set of particles explores the search space, each representing a candidate solution. At each iteration, particles update their position according to three components: inertia (keeping their previous direction), cognitive attraction to their own best historical solution (personal best, pbest), and social attraction to the best solution found in the swarm (global best, gbest). This mechanism allows PSO to balance exploration and exploitation in nonconvex search spaces without requiring gradient information.

In our application, each particle encodes a candidate configuration of contact points

$$\mathcal{P} = \{P_1, P_2, \ldots, P_n\}, \quad P_i \in \mathcal{B},$$

where $\mathcal{B}$ is the boundary of the object. These indices measure, respectively, wrench strength, isotropy, and worst-case controllability.The contact point optimization problem is formulated as a constrained multi-objective optimization:

$$\max_{\mathcal{P}} \quad J(\mathcal{P}) = w_V J_V(\mathcal{P}) + w_I J_I(\mathcal{P}) + w_R J_R(\mathcal{P}) \tag{21}$$

subject to the constraints:

$$\alpha_i > 0, \tag{22}$$

$$|\beta_i| \leq \mu_i \alpha_i, \tag{23}$$

$$\exists \{i, j\} : A_i \cdot A_j < 0 \tag{24}$$

$$\|\mathbf{P}_i - \mathbf{P}_j\| > d_{\min}, \quad \forall i \neq j \tag{25}$$

w_V, w_I, w_R are normalized weighting coefficients and $d_{\min}$ is the minimum separation distance.

For each particle in $\mathcal{P}(m)$, its personal best $p(m)$ is the configuration that has achieved the highest objective value so far. Across the swarm, the best global g is the configuration with the highest objective value among all particles. After each evaluation, if $J(\mathcal{P}(m)) > J(p(m))$, then $p(m)$ is updated. If $J(p(m)) > J(g)$, then g is updated.

The overall progress is summarized in Algorithm 1.

Algorithm 1: PSO-based Contact Placement Optimization

Input: Boundary $\mathcal{B}$, number of contacts n, weights w_V, w_I, w_R, spacing $d_{\min}$, PSO hyperparameters (ω, c_1, c_2)
Output: Optimal configuration $\mathcal{P}^\star = \{P_1^\star, \ldots, P_n^\star\}$

```
Initialize swarm {P(m)} with random placements on B;
Evaluate fitness J(P(m)) for all particles;
Set p(m) ← P(m) and g ← arg max_m J(p(m));
for k = 1 to K do
    foreach particle P(m) do
        Build G, W from P(m) and compute σ1, σ2, σ3;
        Compute indices J_V, J_I, J_R; Evaluate objective J(P(m));
        Check constraints and apply penalty;
        if J(P(m)) > J(p(m)) then
            p(m) ← P(m) ;                          // update pbest
        end
        if J(p(m)) > J(g) then
            g ← p(m) ;                             // update gbest
        end
    end
    Update velocities and positions using PSO rule;
    Project new positions back to B;
end
return g as the optimal configuration P*;
```

4.3 PID Controller with Feasible Wrench Projection

Control Law Design Given optimized contact points, we implement a PID tracking controller to validate the manipulation performance. The control law generates a desired wrench to track the reference trajectory $\mathbf{q}_d(t) = [x_d, y_d, \theta_d]^T$:

$$\mathbf{e}(t) = \mathbf{q}(t) - \mathbf{q}_d(t) \tag{26}$$

$$\mathbf{w}_{\text{des}}(t) = \mathbf{B}\dot{\mathbf{q}}_d(t) - \mathbf{K}_P\mathbf{e}(t) - \mathbf{K}_I \int_0^t \mathbf{e}(\tau)d\tau - \mathbf{K}_D\dot{\mathbf{e}}(t) \tag{27}$$

where $\mathbf{K}_P$, $\mathbf{K}_I$, $\mathbf{K}_D \in \mathbb{R}^{3\times3}$ are diagonal positive definite gain matrices, and $\mathbf{B}$ represents the quasi-static scaling matrix.

Feasible Wrench Projection Since the desired wrench $\mathbf{w}_{\text{des}}$ may not be achievable due to friction and push-only constraints, we project it onto the feasible wrench space $\mathcal{W}_f$ by solving:

$$\mathbf{x}^* = \arg\min_{\mathbf{x}\in\mathbb{R}^{2n}} \|\mathbf{G}'\mathbf{x} - \mathbf{w}_{\text{des}}\|_2^2 \tag{28}$$

$$\text{s.t.} \quad \alpha_i \geq 0, \quad |\beta_i| \leq \mu_i\alpha_i, \quad i = 1, \ldots, n \tag{29}$$

This quadratic programming problem is convex due to the convex nature of the friction cone constraints and the quadratic objective function. The solution $\mathbf{x}^* = [\alpha_1^*, \beta_1^*, \ldots, \alpha_n^*, \beta_n^*]^T$ provides physically realizable contact forces, and the applied wrench is:

$$\mathbf{w}^* = \mathbf{G}\mathbf{x}^* \in \mathcal{W}_f \tag{30}$$

This projection ensures that all applied forces satisfy physical constraints while approximating the desired control action as closely as possible within the feasible wrench space.

5 Results and Discussion

We present the effectiveness of our proposed quality metrics-based contact point optimization framework through comprehensive computational experiments with different object geometries. Optimization performance is evaluated using three distinct object shapes: rectangular , triangular, and pentagonal objects with varying edge lengths, as shown in Fig. 4.

The parameters of the PSO algorithm are configured based on preliminary convergence studies: population size of 50 particles, maximum 100 iterations, inertia weight $w = 0.7$, and acceleration coefficients $c_1 = c_2 = 1.4$. The weighting coefficients for the multi-objective function are set approximately equal ($w_V = w_I = 0.33$, $w_R = 0.34$) to provide balanced optimization across all quality metrics. The force at the contact points ranges from 0-5N.

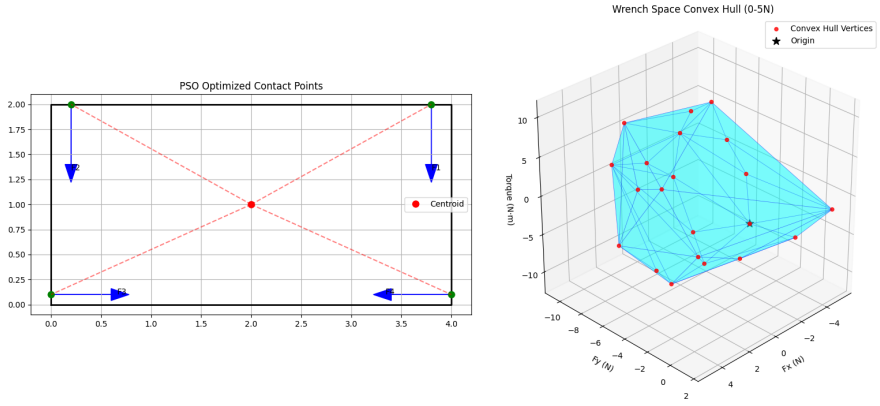

(a) Rectangle

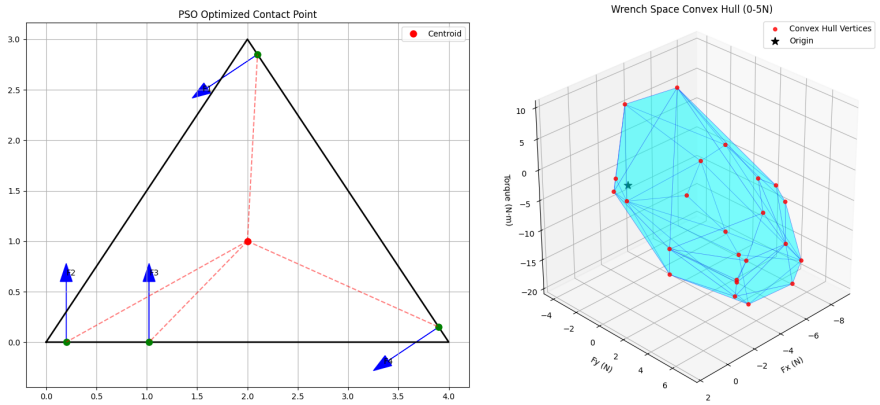

(b) Triangle

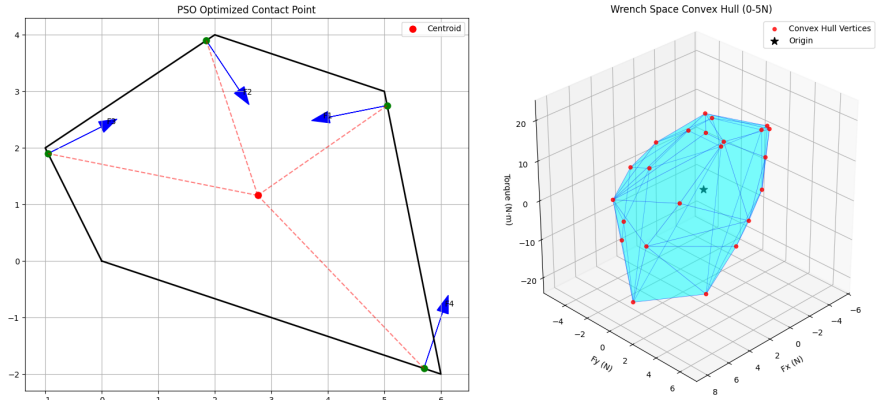

(c) Pentagon

Fig. 4: Results of the search for contact points of different shapes

Figure 4 illustrates the optimized contact placements and the resulting feasible wrench space. On the left, the PSO algorithm selects four contact points located at the corners of the object, symmetrically distributed around the centroid. The pushing directions align with the surface normals, ensuring that forces are applied within the corresponding friction cones. This symmetric configuration minimizes bias in the centroid position and guarantees the generation of bidirectional moments.

On the right, the convex hull of the feasible wrench space is shown in (F_x, F_y, τ) space. The origin lies inside the convex hull, indicating that the system can achieve static equilibrium. Moreover, the large volume of the convex hull demonstrates that the chosen contacts enable the object to generate forces and torques in multiple directions, ensuring both stability and controllability of the manipulation task.

Quantitative evaluation of the optimized placements. For the PSO-optimized contact set, the Gram-based quality indices are: $J_V = 17.0129$, $J_I = 0.2208$, $J_R = 1.9993$, and the combined score $J_{\text{obj}} = 7.4712$. The large volume (J_V) indicates a rich feasible wrench space, while $J_R \approx 2.00$ confirms a strong worst-case capability. The isotropy index $J_I = 0.2208$ reveals directional bias, i.e., the feasible wrench ellipsoid is elongated, so some directions are more controllable than others. This trade-off reflects the chosen weights in the objective: prioritizing overall capacity (J_V) and worst-case robustness (J_R) over uniformity (J_I). If higher directional balance is required (e.g., frequent heading changes), one can increase the weight of J_I during optimization to promote a more isotropic configuration.

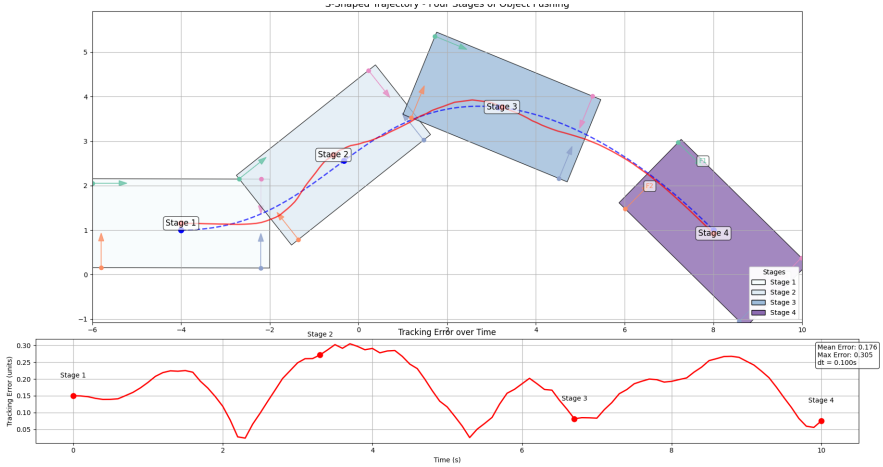

Fig. 5: The process of pushing the tracking object along a given trajectory and the error of the pushing process

Trajectory tracking experiment. Figure 5 illustrates the second experiment, where the object is required to follow an S-shaped reference path. The snapshots at four stages show both the planned trajectory (blue dashed line) and the actual trajectory (red line). The object successfully follows the curved path while maintaining stable pushing contacts.

The lower plot reports the tracking error over time. The mean error is 0.176, and the maximum error is 0.305, both of which remain within a small bound relative to the object size. The error increases temporarily during sharp turns (Stages 2 and 3), where the required wrench approaches the boundary of the feasible wrench space W_f, but remains bounded and quickly decreases afterwards.

These results confirm that the PSO-optimized contact placements provide sufficient controllability for complex curved trajectories. Even with a simple PID controller, the system maintains bounded tracking error under pushing-only constraints. This demonstrates the practical benefit of focusing on force placement optimization: good placements reduce the burden on the controller and enable accurate trajectory tracking without resorting to advanced control schemes such as nonlinear MPC.

6 Conclusion

In this paper, we addressed the problem of pushing-only manipulation by explicitly focusing on optimizing force placements. We introduced three quality indices (J_V, J_I, J_R) derived from the Gram matrix of the grasp map, capturing the volume, isotropy, and worst-case robustness of the feasible wrench space. A Particle Swarm Optimization (PSO) framework was employed to search for contact placements that maximize these indices while satisfying physical constraints such as pushing-only forces, friction cones, and bidirectional moment generation.

After determining the optimized placements, we demonstrated that even a simple PID controller with feasibility projection is sufficient to drive the object along desired trajectories. Simulation results confirmed that the optimized placements lead to stable manipulation and bounded trajectory tracking error, with mean and maximum errors remaining small despite complex S-shaped reference.

These things highlight the importance of the often-overlooked placement phase in object manipulation: By ensuring good contact arrangements up front, the subsequent control task becomes significantly simpler and more robust.

References

1. Bertoncelli, F., Selvaggio, M., Ruggiero, F., Sabattini, L.: Task-oriented contact optimization for pushing manipulation with mobile robots. In: 2022 IEEE/RSJ International Conference on Intelligent Robots and Systems (IROS). pp. 1639–1646 (2022). https://doi.org/10.1109/IROS47612.2022.9982177
2. Ebel, H., Fahse, D.N., Rosenfelder, M., Eberhard, P.: Finding formations for the non-prehensile object transportation with differentially-driven mobile robots. In: Kecskeméthy, A., Parenti-Castelli, V. (eds.) ROMANSY 24 - Robot

Design, Dynamics and Control. pp. 163–170. Springer International Publishing, Cham (2022)
3. Fujisawa, R., Imamura, H., Matsuno, F.: Cooperative transportation by swarm robots using pheromone communication. In: Distributed Autonomous Robotic Systems: The 10th International Symposium. pp. 559–570. Springer (2013)
4. Inglett, J., Rodriguez-Seda, E.: Object transportation by cooperative robots. pp. 1–6 (03 2017). https://doi.org/10.1109/SECON.2017.7925348
5. Kube, C.R.: Task modelling in collective robotics. Autonomous robots **4**(1), 53–72 (1997)
6. Kube, C.R., Bonabeau, E.: Cooperative transport by ants and robots. Robotics and autonomous systems **30**(1-2), 85–101 (2000)
7. Kube, C.R., Zhang, H.: Collective robotics: From social insects to robots. Adaptive behavior **2**(2), 189–218 (1993)
8. Lynch, K.M., Mason, M.T.: Stable pushing: Mechanics, controllability, and planning. The International Journal of Robotics Research **15**(6), 533–556 (1996). https://doi.org/10.1177/027836499601500602, https://doi.org/10.1177/027836499601500602
9. Stüber, J., Zito, C., Stolkin, R.: Let's push things forward: A survey on robot pushing. Frontiers in Robotics and AI **Volume 7 - 2020** (2020). https://doi.org/10.3389/frobt.2020.00008, https://www.frontiersin.org/journals/robotics-and-ai/articles/10.3389/frobt.2020.00008
10. Tang, Z., Feng, Y., Guo, M.: Collaborative planar pushing of polytopic objects with multiple robots in complex scenes (07 2024). https://doi.org/10.15607/RSS.2024.XX.063
11. Tuci, E., Alkilabi, M., Akanyeti, O.: Cooperative object transport in multi-robot systems: A review of the state-of-the-art. Frontiers in Robotics and AI **5** (05 2018). https://doi.org/10.3389/frobt.2018.00059